Computers & Geosciences 56 (2013) 12–22

Contents lists available at SciVerse ScienceDirect

Computers & Geosciences

journal homepage: www.elsevier.com/locate/cageo

A methodology for pseudo-genetic stochastic modeling of discrete fracture networks

François Bonneau [a,c,*], Vincent Henrion [a,c,1], Guillaume Caumon [a,c], Philippe Renard [d], Judith Sausse [b,c]

[a] Université de Lorraine-ENSG, Vandoeuvre-lès-Nancy 54518, France
[b] Université de Lorraine-ENSMN, Nancy 54000, France
[c] Géoressources, UMR 7359, Vandoeuvre-lès-Nancy 54518, France
[d] Centre d'hydrogéologie et de géothermie, Université de Neuchatel, 2000, Switzerland

ARTICLE INFO

Article history:
Received 25 October 2012
Received in revised form
4 February 2013
Accepted 6 February 2013
Available online 24 February 2013

Keywords:
Fracture
Growth
Connectivity
Stochastic simulation
Genetic approach
Pseudo-genetic

ABSTRACT

Stochastic simulation of fracture systems is an interesting approach to build a set of dense and complex networks. However, discrete fracture models made of planar fractures generally fail to reproduce the complexity of natural networks, both in terms of geometry and connectivity. In this study a *pseudo-genetic* method is developed to generate stochastic fracture models that are consistent with patterns observed on outcrops and fracture growth principles. The main idea is to simulate evolving fracture networks through geometric proxies by iteratively growing 3D fractures. The algorithm defines heuristic rules in order to mimic the mechanics of fracture initiation, propagation, interaction and termination. The growth process enhances the production of linking structure and impacts the connectivity of fracture networks. A sensitivity study is performed on synthetic examples. The method produces unbiased fracture dip and strike statistics and qualitatively reproduces the fracture density map. The fracture length distribution law is underestimated because of the early stop in fracture growth after intersection.

1. Introduction

Fractures are ubiquitous structures occurring in a wide variety of rock types and tectonic settings over a broad range of scales. The average permeability of these structural heterogeneities may be a few orders of magnitude higher or lower than those of the surrounding matrix rocks. Consequently, fractures are known to significantly impact fluid flows.

Because the spatial characteristics of a fracture network cannot be known deterministically, they are simulated using a statistics measured field. The high uncertainty of model geometry requires simulating several networks. A lot of methods generating stochastic fracture networks have been developed (for reviews, see e.g. Jing, 2003; Chilès, 2005; Dershowitz et al., 2004; Dowd et al., 2007). To be consistent with field observations, the statistical process can be constrained by 3D density and orientation maps derived from seismic attributes (Dershowitz, 1984; Maerten et al., 2000; Will et al., 2004; Freudenreich et al., 2005) and/or strain analysis (Priest and Hudson, 1976; Kloppenburg et al., 2003). Discrete fracture network (DFN) models generally assume planar and rectangular fractures. Unlike geomechanical fracture models reproducing fracture growth and interaction (Olson, 1993; Renshaw and Pollard, 1994b; Tuckwell et al., 2003; Jing, 2003; Welch et al., 2009), planar discrete fracture models cannot reproduce linking structures and tend to underestimate the connectivity of the fracture network for a given fracture density.

We propose a *pseudo-genetic* approach for simulating 3D DFN models. It integrates insights from fracture mechanics within a probabilistic framework. As proposed by Gringarten (1998), Bourne et al. (2000), Hoffmann et al. (2004) and Srivastava et al. (2005), we aim at minimizing the weakness of both mechanistic and probabilistic approaches while exploiting their strengths. We are particularly interested in reproducing the effect of mechanical interactions between fractures and in investigating the resulting fracture network connectivity.

The *pseudo-genetic* method focusses on tensile fractures (Mode I). Such fractures are grown starting from a prior knowledge of fracture parameters and of rules about fracture initiation, propagation and termination. As recalled in Section 2, a tensile fracture creates symmetrical constraint accumulation zones (Fig. 1) and

* Corresponding author at: Université de Lorraine, CNRS, CREGU ENSG, Campus BRABOIS, TSA 706 cedex, France. Tel.: +333 83 59 64 56; fax: +333 83 58 64 60.
E-mail addresses: bonneau@gocad.org (F. Bonneau), vincent.henrion@total.com (V. Henrion), Guillaume.Caumon@univ-lorraine.fr (G. Caumon), Philippe.Renard@unine.ch (P. Renard), judith.sausse@mines.inpl-nancy.fr (J. Sausse).
[1] Presently at Total SA, CSTJF, avenue Larribau, F-64000 Pau, France.

0098-3004/$ - see front matter © 2013 Elsevier Ltd. All rights reserved.
http://dx.doi.org/10.1016/j.cageo.2013.02.004

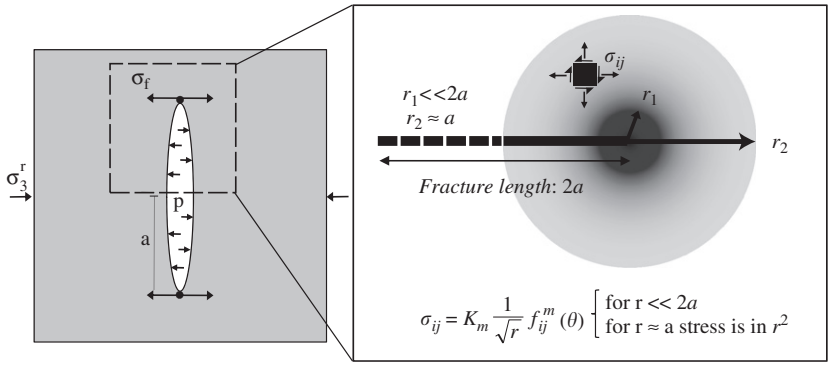

Fig. 1. Simplified representation of the stress concentration around fracture tips. (r,θ) are polar coordinates at the fracture tip, $f(\theta)$ is a function determined by the strain tensor and is independent of geometric or mechanic parameters. K_m is the stress intensity factor for each displacement mode: m=I, II, III (modified from Pollard and Aydin, 1988).

grows parallel to the crack plane. Rock heterogeneities (flaws, pre-existing fractures, etc.) alter the propagation path loading the fracture with a mixed mode I–II (Renshaw and Pollard, 1994b; Vermilye and Scholz, 1998). Srivastava et al. (2005) use empirical geostatistical rules inspired by geomechanics to grow fractures and fill in 2D and 2.5D fracture maps. In the same manner, we use heuristic geometric rules to mimic mechanical fracture growth and simulate 3D DFNs (Section 3). The simulation method generates realistic fracture patterns in 3D with less computational efforts than geomechanical simulation. The method produces multiple realizations of fracture systems by randomly sampling input statistical data then growing each fracture using deterministic heuristic rules. In Section 4, we show the impact of the method on the connectivity and statistics of the DFN as compared to classical planar DFNs.

2. Physics of fracture growth

The simulation technique proposed in this paper is a *pseudo-genetic* approach which propagates fracture patterns using heuristic rules for fracture growth instead of mechanical calculations. In order to illustrate the underlying ideas that lead to the definition of these rules, we summarize below some important concepts and results about fracture growth in the framework of Linear Elastic Fracture Mechanics (LEFM). We refer the interested reader to Atkinson (1982), Pollard and Aydin (1988) and Atkinson and Craster (1995), and references therein.

2.1. Fracture initiation

Fractures initiate at flaws for instance, fossils, grains, cavities, micro-cracks and other objects, that have elastic properties different from those of the surrounding rock. These flaws modify the stress field in such a way that the magnitude of local stresses at the flaw may exceed the strength of the rock, thereby initiating fractures (Fig. 1). We reproduce this process using a heterogeneous Poisson point process for fracture seeding. The fracture density cube may come for instance from structural analysis or microseismic data (Macé, 2006; Amorim et al., 2012). As the stress concentration around fracture tips increases with the fracture area, a fracture continues to propagate as long as there is energy available for propagation.

2.2. Fracture propagation

The propagation of a fracture is controlled by the stress field near fracture tips. This stress field is heterogeneous, the region of stress concentration is small and the stresses decrease with the distance to the tip (Fig. 1). When the fracture propagates a damage zone appears relaxing the constraints around. The zone where constraints are relaxed is called the *shadow zone* (Scholz et al., 1993; Cowie and Shipton, 1998; Vermilye and Scholz, 1998; Kim et al., 2004).

All stress components σ_{ij} around the fracture are proportional to quantities called *stress intensity factor* (K_m) (Pollard and Aydin, 1988). They measure the stress concentration which depends on the applied load and on the fracture geometry (Fig. 1). In fracture mechanics, three loading modes are generally identified (Pollard and Aydin, 1988):

- mode I: tensile mode which characterizes opening displacement;
- mode II: shearing mode which characterizes sliding perpendicular to the fracture propagation front;
- mode III: shearing mode which characterizes sliding parallel to the fracture propagation front.

A tensile fracture propagates when the mode I stress intensity factor (K_I) reaches a critical value for mode I loading (K_{IC})

$$K_I > K_{IC} \tag{1}$$

where K_{IC} is called the fracture toughness and is a property of the material. Expressions for stress intensity factor combined with the propagation criterion allow one to make important inferences about the behavior of fractures:

- For two fractures of unequal areas subjected to the same driving stress, the larger joint will meet the propagation criterion first.
- For joints with equal areas in a spatially varying stress field, the joint subjected to the greatest driving stress will propagate first.

In the proposed simulation, the stress intensity factor is not modeled explicitly but the observations about fracture sizes are directly translated in the growth algorithm.

2.3. Fracture interaction

Interactions between nearby fractures influence fracture growth and termination, and consequently the fracture pattern. A fracture propagates if K_I increases (when constraint accumulation zones overlap) and/or if K_{IC} decreases (when a fracture is growing in the damage zone) (Eq. (1)). Each fracture enhances the

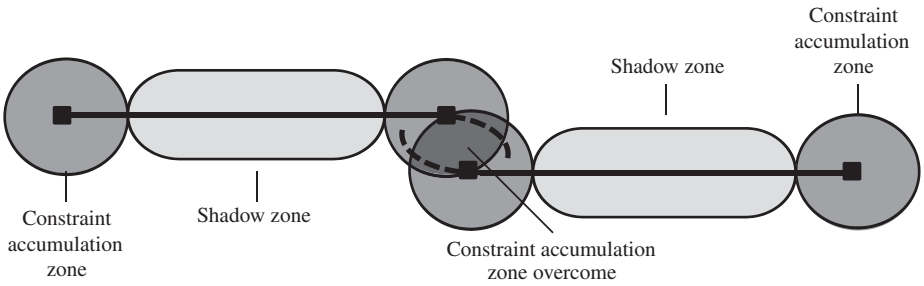

Fig. 2. Interaction between close fractures forces their propagation paths to converge towards each other. This has a significant effect on the connectivity of the fracture pattern which in turn is expected to have a first-order impact on flow (modified from Kim et al., 2004).

propagation of its neighbor by inducing shear stress. As a result, fractures progressively converge towards each other and enhance fracture linkage. This explains the common hooked-shape of en-echelon fractures (Fig. 2). Fracture interactions have an important impact on the final geometry of the fracture network.

As the area ratio between the two interacting fractures increases, the propagation energy of the largest fracture approaches that of an isolated fracture, while the energy for the shorter fracture falls to zero. This means that the longer fracture deactivates the growth of nearby shorter fracture. DeGraff and Aydin (1987) reported a similar shielding effect when parallel fractures interact. The shielding effect is taken into account in the proposed simulation algorithm which iteratively grows fractures.

2.4. Fracture termination

Fracture termination depends on the factors that decrease or increase the energy available for propagation. Because stress concentration at tips increases with fracture length, a fracture should not stop growing if all other factors remain constant. Fracture propagation stops if either the fluid pressure decreases, or if remote stresses increase sufficiently. Fracture termination may also occur depending on rock properties, for example, when a fracture propagates into a stiffer or a less compressible rock, or when a fracture intersects another discontinuity such as lithologic boundary, or another fracture (Cooke and Underwood, 2001; d'Alessio and Martel, 2004). In our approach these effects are addressed through the input statistical law for fracture size, and by terminating fractures during propagation rather than through a post-processing (Macé, 2006).

3. Pseudo-genetic simulation of fracture network

The key aspect of the *pseudo-genetic* simulation of fracture network is to replace mechanical calculations by heuristic rules based on mechanical principles that govern opening fracture growth. We consider that the curvature observed for mode I fracture network is mainly due to the growth of neighboring fractures. We explain the fracture growth algorithm for 2D fracture network, then discuss extensions to 3D cases.

3.1. Initial fractures

Srivastava et al. (2005) propose to initiate fractures using a clustered point process around cracks identified from aerial photography. Here, we initialize fracture seeds using a traditional Poisson point process (Stoyan et al., 1995). Micro-cracks are randomly distributed according to a density model (expected number of fractures per unit volume). As in Srivastava et al. (2005), the fractures are not generated in their final state but as short linear segments (in 2D) which are then propagated. The orientations of fracture are given by a statistical distribution law or by an orientation map. Such local orientation may come from seismic attributes (Dershowitz, 1984; Will et al., 2004; Freudenreich et al., 2005) or prior geological constraints and deformation analysis (curvature, strain) (Priest and Hudson, 1976; Kloppenburg et al., 2003; Macé et al., 2004). An intended final fracture length is also drawn in a distribution law. From the expected final length (L_f) and the number of propagation steps (k) fixed by the user, the initial length (l_i) of the fracture is computed as follows:

$$l_i = L_f/(2k+1) \tag{2}$$

The number of propagation steps directly controls the initial fracture length and growth speed. Fixing the number of propagation steps to 0 means that fractures get directly to their final state. It corresponds to the classical simulation of a discrete fracture network without propagation.

3.2. Propagation process

Once fractures have been initialized, their propagation is simulated by sequential growth. Each fracture of the network is grown by decreasing sizes. Longer fractures are first propagated to reproduce the effect of differential growth rate among fractures (i.e. a few large fractures have the greatest impact on the final fracture pattern (see Section 2.2)). Indeed, longer fractures having their process zones growing rapidly will affect the propagation of smaller fractures.

Both constraint accumulation and shadow zones of fractures act on the growth of neighboring fractures (Section 2.2). The physical controls on the size of these zones are poorly understood. Estimates range from 10% to 50% of the fracture dimension (Cowie and Shipton, 1998).

In our implementation, an attraction zone distance (d_{At}) is defined around each fracture to reproduce the effect of these zones. The attraction zone is represented by a sphere centered on the closest node to the fracture tip to propagate. The attraction zone distance (d_{At}) (radius of the sphere) is computed from a ratio (r fixed by the user) of the corresponding fracture area (A):

$$d_{At} = \sqrt{A/(\pi \times r)} \tag{3}$$

The search strategy to define interacting fractures with the current growing fracture is illustrated in Fig. 3. For a free fracture tip, the space is separated by the plane normal to the current direction of propagation. All fractures located ahead of the defined plane are browsed to check if there is an overlap between the attraction zone of the fracture being propagated and the surrounding fracture attraction zone. At this point, our implementation does not distinguish between the constraint

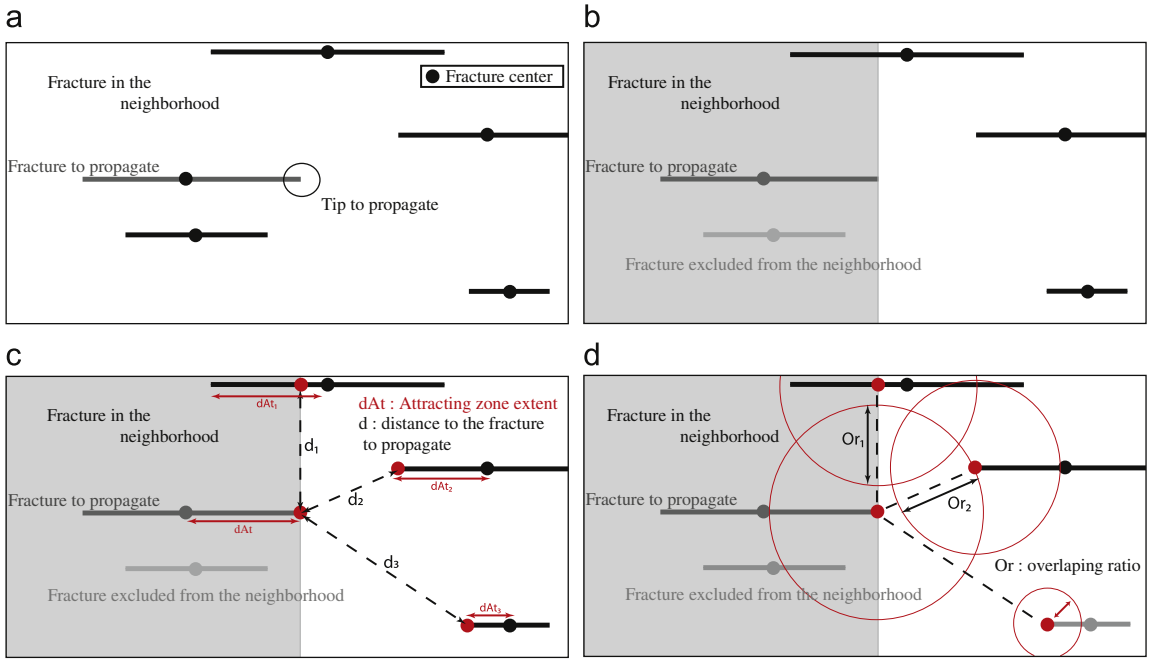

Fig. 3. Fracture neighborhood definition – considering an initial fracture neighborhood (a), two exclusion steps select fractures which will drive its propagation. The first one (b) aims at excluding fractures which are behind of the fracture tip to propagate. The second one check the overlaps between neighboring fracture attractive zones (d). The size of attractive zone is computed as a ratio (r) of the fracture area (c) (see Eq. (3), here $r=2$).

accumulation zone and the shadow zone of neighboring fractures. A very simple way to achieve this is to stop fracture propagation when it enters the shadow zone of another fracture.

For each fracture, its free tips are propagated by a fixed step length (l_i in Eq. (2)). The direction of propagation ($\overrightarrow{P}$) depends on: (1) the possible interactions between the extremity being propagated and nearby fractures ($\overrightarrow{I}$) and (2) the background orientation ($\overrightarrow{O_b}$). The influence of each component is controlled by a weighting factor (λ_0) (Fig. 5(d)):

$$\overrightarrow{P} = ((1-\lambda_0)\cdot \overrightarrow{I} + \lambda_0 \cdot \overrightarrow{O_b}) \cdot l_i \tag{4}$$

The background orientation ($\overrightarrow{O_b}$ in Eq. (4)) takes into account both the fracture mechanical inertia through the current propagation vector ($\overrightarrow{P_{cur}}$) and possibly a local orientation map ($\overrightarrow{O_m}$), if any. The current growth direction of the fracture is adjusted considering an optional orientation map by a weighting factor defined by the user (ξ_0) (Fig. 5(c))

$$\overrightarrow{O_b} = (1-\xi_0)\cdot \overrightarrow{P_{cur}} + \xi_0 \cdot \overrightarrow{O_m} \tag{5}$$

The deviation ($\overrightarrow{I}$) is computed as the mean orientation of the vectors linking the extremity being propagated and the closest points of the fractures contained in the neighborhood. These linking-vectors are noted $\overrightarrow{D_i}$ (Fig. 5(a)). Srivastava et al. (2005) use a distance-based technique weighted by a kriging approach to define the contribution of each linking-vector in the computation of the mean deviation vector. Considering that fracture curvature is mainly due to the fracture interaction stress (Renshaw and Pollard, 1994a), we introduce weight linking-vectors ($\overrightarrow{D_i}$) by an inverse distance weighting ratio (λ_i) (Fig. 3(c) and (d)):

$$\overrightarrow{I} = \sum_i \lambda_i \overrightarrow{D_i} \quad \text{with } \lambda_i = (Or_i/d_i)/\sum_j (Or_j/d_j) \text{ and } Or_i = d_{At} + d_{Ati} - d_i \tag{6}$$

For each interacting fracture, the overlapping ratio (Or_i) quantifies the extent of the overlap between attracting zones. Then an inverse distance interpolation weighted by Or_i sets the impact of interacting fracture on the growth.

Finally, the free tip is propagated by its fixed step size (l_i see Eq. (2)) in the new direction of propagation. Propagation vectors ($\overrightarrow{P}$ in Eq. (4)) are computed and applied at each fracture tip to evaluate new ones. New line segments (in 2D) or new surface elements (in 3D) are created between old and new tips.

3.3. Fracture termination

Fracture propagation stops when the fracture reaches its intended final length (i.e. at the maximum number of propagation steps) or when it intersects another fracture or another discontinuity such as a bedding plane. It is also possible to allow crossings. Therefore a truncation probability is used to control the proportion of fractures which terminate on pre-existing mechanical discontinuities. Stopping fractures propagation does not guarantee that the output length distribution exactly matches the input one. This also happens in classical DFN approaches when fractures are post-processed to respect a given hierarchy. We will quantify the bias on fracture length in Section 4. It is however important to note that the sizes of the fractures are often very uncertain since borehole data provides only indirect information and analogs may not be available.

3.4. Extensions to 3D

The application of the method in 3D is based on a description of fractures as rectangles. The best results are obtained using a 2.5D approach for each fractures in which the 2D algorithm is applied along strike and the fracture is extrapolated linearly in the dip direction. Our experiments applying the same propagation rules in both strike and dip directions often yield fractures which have a saddle geometry (Gaussian curvature <0) (Fig. 4(b)).

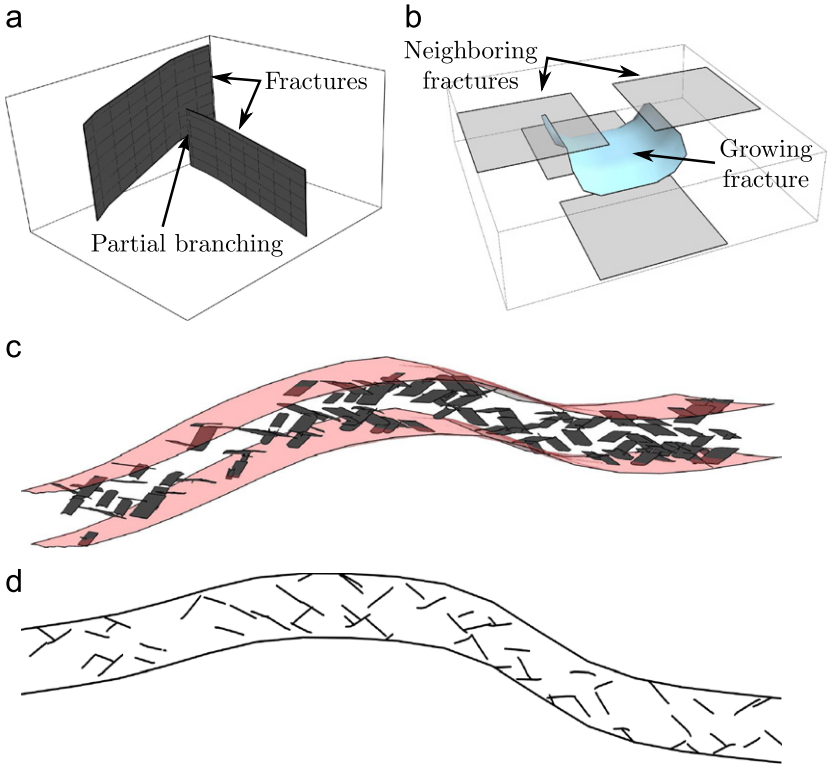

Fig. 4. 3D DFN and saddle geometries – a 3D DFN made of two sets of fractures has been grown in a single layer using the *pseudo-genetic* algorithm. (c) presents a 3D view and (d) presents fracture traces on a cross-section. Because every fractures are in the same layer, we reduce the proportion of partial branching (a) and fracture with negative Gaussian curvature (b).

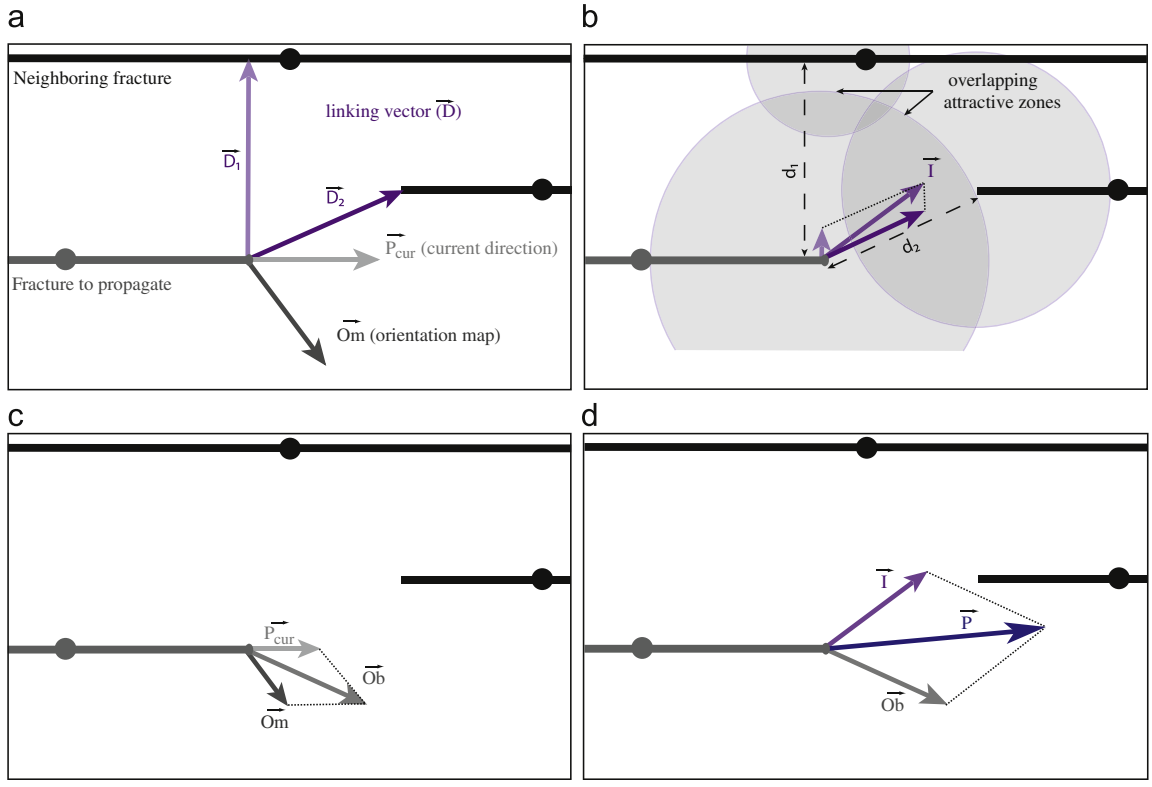

Fig. 5. Propagation vector computation – the propagation vector is a linear combination of a set of vectors (a). Its two main components are the deviation vector (b) and the local stress field vector (c). The deviation vector is computed by resizing the linking vector (Eq. (6)).

Another open problem in 3D is the partial branching of fractures, whereby two fractures intersect only a part of the total fracture edge (Fig. 4(a)). In that case it is possible to stop the propagation once the contact is detected.

For these reasons, we consider the algorithm best works when all fractures are seeded in the same layer (Fig. 4(c) and (d)).

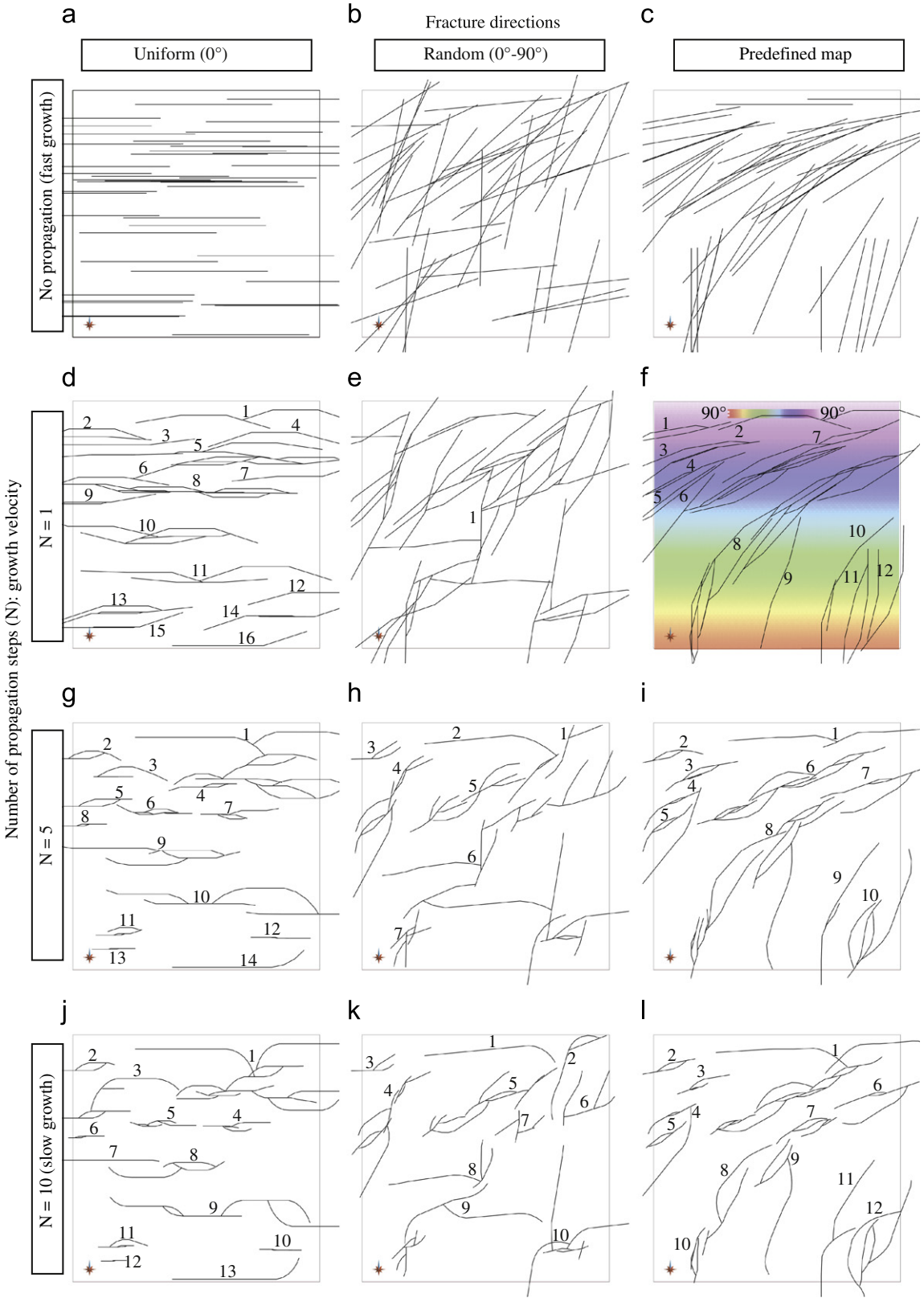

Fig. 6. Sensitivity to growth velocity – tests have been performed running the *pseudo-genetic* method on a horizontal layer with a homogeneous fracture density map. For each fracture, the attraction zone size is set to 33% of the effective fracture size ($r=3$, Eq. (3)) and the coefficient controlling the influence of the background orientation (λ_0, Eq. (4)) has been set to 0.75.

4. Examples and sensitivity analysis

The *pseudo-genetic* method sets the global DFN geometry with statistics and calibrates it locally using a fracture growth process. The growth offers three different input parameters which control the fracture geometry:

- The fracture growth velocity (set by the number of propagation steps N).
- The weight of the background orientation vector (set by the weighting factor λ_0, Eq. (4)).
- The attraction zone extent (set by the ratio r, Eq. (3)).

An infinite number of different networks can be generated with the described set of parameters (input statistics and growth parameters). We describe the effect of growth parameters on fracture geometry by selecting few values for each parameter N, λ_0 and r. We consider the corresponding DFN properties qualitatively and quantitatively.

4.1. DFN qualitative study: 2D-Example

In this part, visual criteria are used to describe output DFN geometries. We particularly focus on fracture length, bending, and on the number of clusters. Fig. 6(a)–(c) shows fracture networks obtained by classical DFN simulations (without growth), which is our reference case to study the effect of fracture growth on input statistics and fracture clustering. Fig. 6(a) shows a DFN made of parallel planar fractures with no connection. This is unrealistic regarding the fracture growth principles described in Section 2. On the contrary, Fig. 6(b) and (c) shows DFNs for which almost all fractures are connected to at least another fracture. Those are not realistic either because fracture geometry is set independently for each fracture without considering any interactions between fractures. A lot of fractures are intersecting one or several others without being affected.

Increasing the number of propagation steps (N) leads to an increase in the number of times the fracture interactions are evaluated. Fig. 6(d), (g) and (j) shows how N impacts the fracture geometry on a planar DFN with a constant orientation. When N

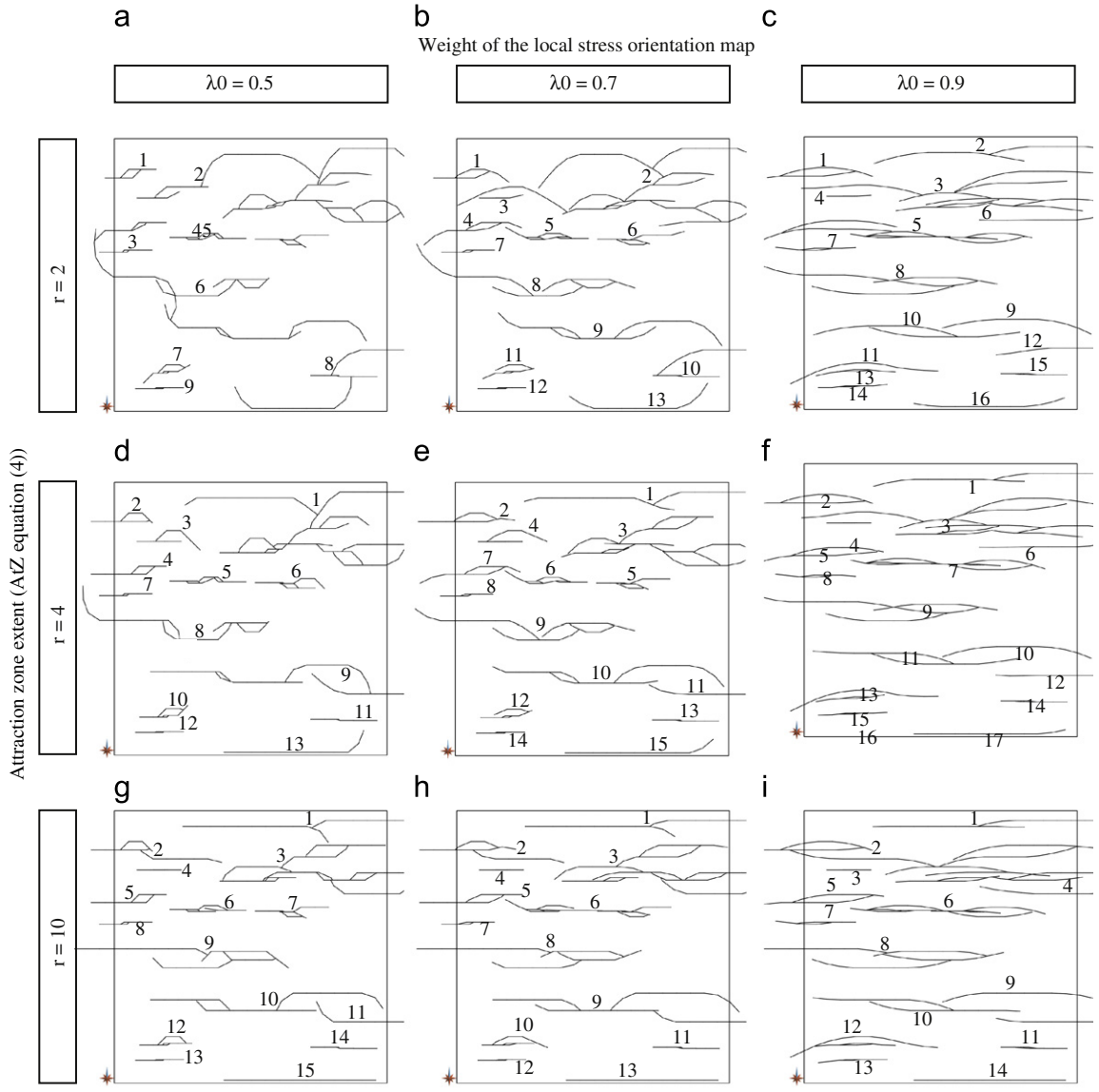

Fig. 7. Sensitivity to the attraction zone size and to the local orientation factor (λ_0, Eq. (4)) – tests have been performed running a five-propagation-step simulation with a uniform direction and a homogeneous fracture density map.

increases, fracture bending increases as well as fracture interconnections. Thus, the number of clusters decreases. In Fig. 6(e), (h), (k) and (f), (i), (l), an increase of N has the same effect on fracture bending, but the number of clusters tends to increase when compared to planar DFNs. This can be explained because we stop fracture growth when the fracture is branching on another one. Then, one fracture cannot cross several fractures.

The number of propagation steps (N) influences fracture interactions. Fracture deviation is computed at each propagation step, so deviation effects compound. As a result, fracture geometries may be strongly curved with high value of N. Fig. 7 further explores the effect of attraction zone extent (r), and the weighting factor setting the influence of these fractures in the deviation computation (λ_0). When r increases, the deviation is computed from closer fractures reducing curvature of fractures and changing the overall connectivity of the network for fixed fracture centers. When λ_0 increases, the deviation effect is reduced, leading to more linear fractures.

From Figs. 6 and 7, we can observe that growth parameters impact fracture bending and branching. A branching contact between two fractures stops the growth. As a consequence, fracture length is reduced, the number of fractures per cluster increases and the number of clusters decreases.

4.2. DFN quantitative study

The algorithm parameters have a direct impact on the fracture network emergent parameters such as connectivity or size of non-fractured blocks. Over a large number of DFN realizations, it is possible to quantify how such fractures evolve with input growth parameters. Therefore, we have generated three different kinds of DFNs and compared their statistics on hundred realizations. Each DFN is composed of vertical fractures simulated on a homogeneous fracture density map and constrained by input parameters as summarized in Table 1. The order of magnitude spanned by distributions of natural fracture network is very large (e.g. 10–100 m). In these examples, we chose a narrow uniform length distribution law (from 15 to 35 m) to perform a visual study of fracture interactions.

Table 1
DFN simulation parameters.

Case	Method	Azimuth distribution	Length distribution	Number of growth steps	λ_0 (Eq. (4))	Attraction zone ratio
1	Planar	Uniform (80–100°)	Uniform (15–35 m)	–	–	–
2	Pseudo-genetic			5	0.9	4
3	Pseudo-genetic			5	0.7	2

Table 2
DFN statistics.

Case	Total number of fractures	Average number of clusters per DFN	Average number of intersections per fracture I_f	Mean fracture length (m)	Percolation parameter (p)
1	642	609	0.05	25.0	6.42
2	642	298	1.15	19.5	3.90
3	642	191	1.70	15.6	2.50

4.2.1. Quantitative study of fracture properties

Statistics on DFN properties evaluated from cases 2 and 3 (Table 1) are compared to those from classical DFN simulation which perfectly honors input statistics (case 1, Table 1). Fig. 9 and Table 2 gather the results of the three different cases in terms of fracture (length, azimuth) and fracture network parameters (average number of clusters per DFN, connectivity). The bending of fractures slightly spreads input azimuth distribution but the principal direction is kept (Fig. 9(c)). The main impact of the method is to decrease the length of fracture because of the growth inhibition due to fracture interactions (Fig. 9(b) and (c)). We observe that this bias of length is higher when the range of the input length distribution is wider. A possible strategy to alleviate this truncation effect could be to continue the propagation of lager fractures when they intersect smaller ones.

Because the *pseudo-genetic* method changes the fracture length distribution (creating smaller fractures), it is worth checking the fracture density map for possible bias. The DFNs presented here are simulated from a homogeneous fracture density map, and should therefore reproduce a random object implantation (Stoyan et al., 1995), and E-types obtained from *pseudo-genetic* simulations should be homogeneous. Three thousand simulations have been performed for each case (Table 1) and the E-types were built (Fig. 8) by rasterizing each fracture trace on the Cartesian grid and computing the experimental probability for each grid cell to be intersected by a fracture. They show that the method reproduces a homogeneous fracture density map. However, the density values observed for the E-type of planar DFNs (Fig. 8(a)) are higher than the ones obtained with the *pseudo-genetic* method (Fig. 8(b) and (c)). To reduce this bias we are working on a method in which fractures will be implanted and grown until the expected density is reached.

4.2.2. Quantitative study of fracture connectivity

Connectivity is a crucial parameter to investigate because of its direct impact on fluid flow. It can be defined locally as a two point connectivity (Renard et al., 2011) or at global scale following the percolation concept. Robinson (1983, 1984) found that the right

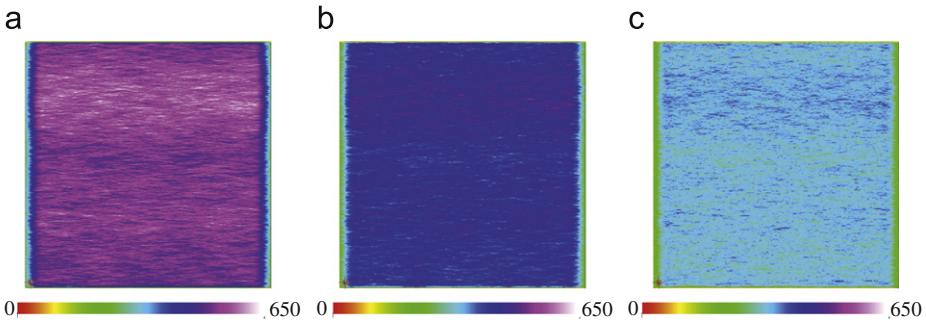

Fig. 8. E-types built from 3000 DFN simulations (a) case 1, (b) case 2 and (c) case 3.

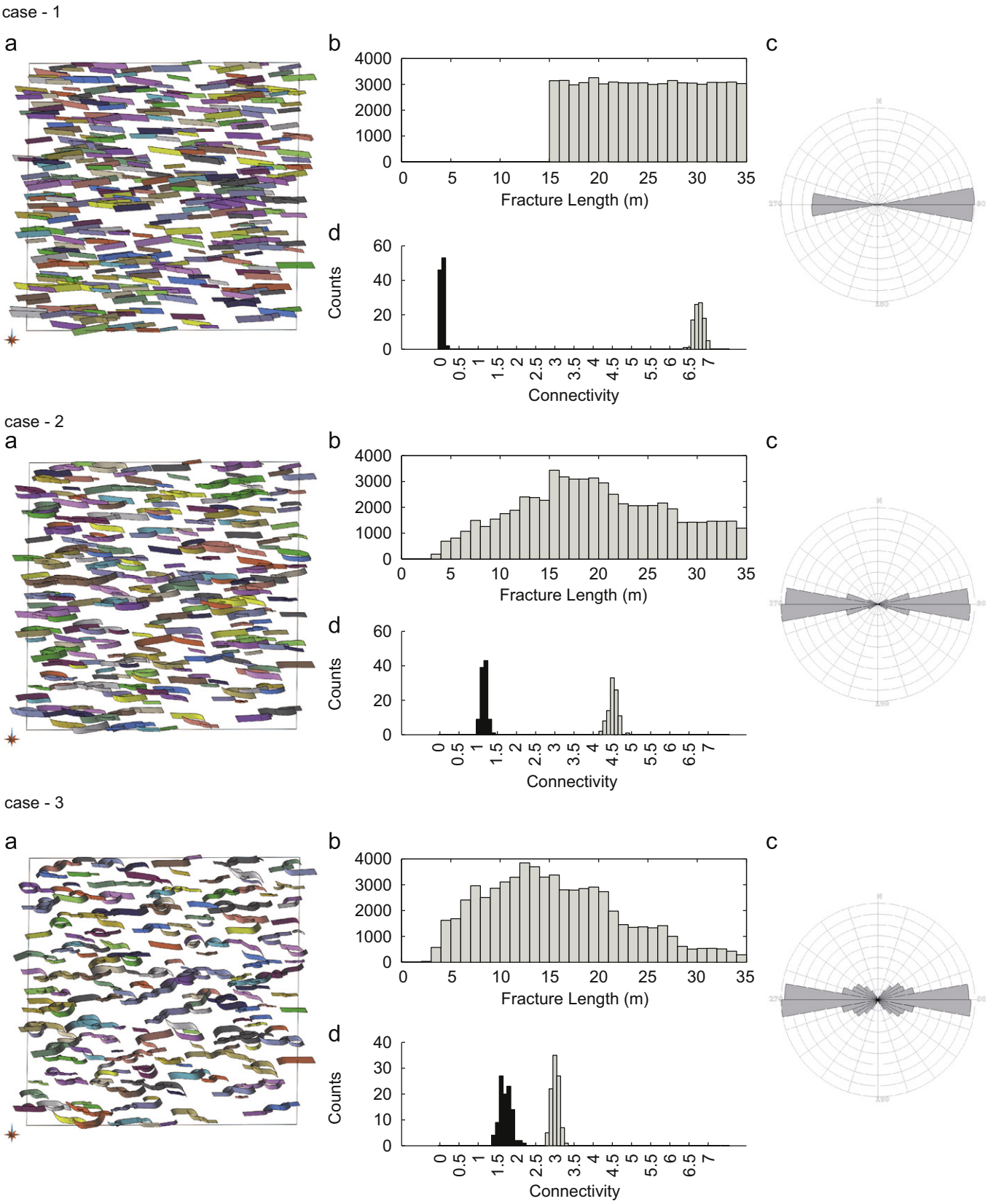

Fig. 9. DFN quantitative study. Three sets of one hundred DFNs have been simulated, from input data given in Table 1. For each of the three cases (a) shows the geometry of the clusters (highlighted by the color map) and the fractures in one DFN; (b) shows statistics on fracture length; (c) shows statistics on fracture azimuth and (d) shows statistics on connectivity. The black distribution illustrates the average number of intersections per fracture (I_f) and the gray one illustrates the percolation parameter (p). Fracture length decreases when the number of clusters decreases. The number of intersections per fracture and so the number of fractures per cluster increases with fracture bending, whereas the percolation parameter tends to decrease because of the growth inhibition due to fracture interactions. Compared to planar DFNs, those generated by the *pseudo-genetic* method do not reproduce perfectly input statistics, but the number of interconnections between fractures underline a higher connectivity. (For interpretation of the references to color in this figure legend, the reader is referred to the web version of this article.)

invariant to quantify the fracture network connectivity is the average number of intersections per fracture I_f (Table 2). He computes a percolation threshold of approximatively 3.6 intersections per fracture. This result has been computed independently of any orientation anisotropy. It means that even if the fracture network presents a preferred strike or orientation, if the average number of intersections per fracture exceeds 3.6, at least one connected fracture swarm crosses the model. Bour and Davy (1997, 1998) propose a unique percolation parameter p (Eq. (7)) to describe the network connectivity

$$p = \left(\sum_{i=1}^{n} l_i^3\right)/V \tag{7}$$

where n is the total number of fractures in the network, l_i the fracture length and V the volume of the system. The parameter p represents the effective connectivity of the network. The proportion of fractures inside the volume of interest is evaluated. Considering planar fractures with random orientations, Bour and Davy (1998) define a length and a density parameter to fix an effective connectivity. Bour and Davy (1997, 1998) compute the percolation threshold which has to be calibrated for a non-random strike distribution law.

Table 2 quantifies the network connectivity for the cases presented in Table 1. For each case, we start from the same length distribution law, fracture density map, and seed to initialize the Poisson point process. As a consequence, the same number of fractures is simulated. For cases 1–3 parameters are set in order to increase the fracture bending. This also reduces the number of clusters and increases the average number of intersections per fracture I_f. Compared to planar DFN simulation, the *pseudo-genetic* method considerably increases fracture intersection probability and creates DFNs closer to the percolation threshold proposed by Robinson (1983, 1984). However, we observe a diminution of the percolation parameter (p) when the number of connections per fracture increases. This is due to the linking process that stops the growth process and underestimates both the length distribution law and the fracture density map.

In a fracture network, both the number of connections and the fracture density have an impact on the connectivity. De Dreuzy et al. (2001) and Davy et al. (2010) perturb fracture length distribution law and density parameters to enhance fracture interconnections and so rock permeability. Our method allows an increase in interconnections even if we simulate fractures with preferred orientation. The early stop of fracture growth brings bias to the length distribution law and the fracture density map. We are currently working on this problem because it impacts connectivity and fluid flow.

5. Conclusion

A stochastic approach enables the building of a large set of DFN constrained by statistics from field observations. It is difficult to characterize these models because we have no algebraic parameters to quantify DFN quality. In this work we test how simulated DFN honor conditioning data, particularly by considering fracture parameters distribution law. Our method relies on a *pseudo-genetic* simulation to generate DFNs. It increases the consistency with natural analogs but does not perfectly honor conditioning statistics. However, the huge uncertainties associated to input statistics justify their approximation. In the spirit of Barbier et al. (2012) who propose a parameter to characterize fracture spacing, new tools have to be implemented to improve DFN characterization. Most of the authors propose the assumption of planar fractures. This underestimates the proportion of linking structures and acts on DFN parameters especially in terms of connectivity and flow. However, we have shown that taking albeit approximately the fractures interaction and sinuosity into account has a significant impact on connectivity measures. The natural reservoir connectivity is difficult to estimate and to use as conditioning data.

That is why an important further step would be to calibrate parameters with dynamic data.

Finally, more research needs to incorporate genetic concepts in DFN simulation to bridge the gap between approaches in characterization of fractured rocks.

Acknowledgments

The authors are grateful to the academic and industrial sponsors of the Gocad Consortium managed by ASGA (Association Scientifique pour la Géologie et ses Applications) for funding this work, and to Paradigm Geophysical for providing the Gocad software and API. We would also like to thank reviewers for constructive comments which helped improve this paper. This work was performed in the framework of the "Investissements d'avenir" Labex RESSOURCES21 (ANR-10-LABX-21).

References

Amorim, R., Boroumand, N., Vital Brazil, E., Hajizadeh, Y., Eaton, D., Costa Sousa, M., 2012. Interactive sketch-based estimation of stimulated volume in unconventional reservoirs using microseismic data. In: ECMOR XIII-13th European Conference on the Mathematics of Oil Recovery.

Atkinson, B., 1982. Subcritical crack propagation in rocks: theory, experimental results and applications. Journal of Structural Geology 4 (1), 41–56.

Atkinson, C., Craster, R., 1995. Theoretical aspects of fracture mechanics. Progress in Aerospace Sciences 31, 1–83.

Barbier, M., Hamon, Y., Callot, J., Floquet, M., Daniel, J., 2012. Sedimentary and diagenetic controls on the multiscale fracturing pattern of a carbonate reservoir: the Madison formation (Sheep Mountain, Wyoming, USA). Marine and Petroleum Geology 29 (January (1)), 50–67.

Bour, O., Davy, P., 1997. Connectivity of random fault networks following a power law fault length distribution. Water Resources Research 33, 1567–1583.

Bour, O., Davy, P., 1998. On the connectivity of three-dimensional fault networks. Water Resources Research 34 (10), 2611–2622.

Bourne, S., Brauckmann, F., Rijkels, L., Stephenson, B., Weber, A., Willemse, E., 2000. Predictive modelling of naturally fractured reservoirs using geomechanics and flow simulation. In: The Ninth Abu Dabi International Petroleum Exhibition and Conference (ADIPEC 0911), pp. 1–10.

Chilès, J., 2005. Stochastic modeling of natural fractured media: a review. In: Leuangthong, O., Deutsch, C.V. (Eds.), Geostatistics Banff 2004 of Quantitative Geology and Geostatistics, vol. 14. Springer, pp. 285–294.

Cooke, M., Underwood, C., 2001. Fracture termination and step-over at bedding interfaces due to frictional slip and interface opening. Journal of Structural Geology 23, 223–238.

Cowie, P., Shipton, Z., 1998. Fault tip displacement gradients and process zone dimensions. Journal of Structural Geology 20 (8), 983–997.

Davy, P., Le Goc, R., Darcel, C., Bour, O., De Dreuzy, J., Munier, R., et al., 2010. A likely universal model of fracture scaling and its consequence for crustal hydromechanics. Journal of Geophysical Research B: Solid Earth 115, B10411.

De Dreuzy, J., Davy, P., Bour, O., 2001. Hydraulic properties of two-dimensional random fracture networks following a power law length distribution: 2. Permeability of networks based on lognormal distribution of apertures. Water Resources Research 37 (8), 2079–2095.

DeGraff, J., Aydin, A., 1987. Surface morphology of columnar joints and its significance to mechanics and directions of joint growth. Geological Society of America Bulletin 99, 607–617.

Dershowitz, W., 1984. Rock Joint Systems. Ph.D. Thesis, Massachusetts Institute of Technology, Cambridge.

Dershowitz, W., La Pointe, P., Doe, T., et al., 2004. Advances in discrete fracture network modeling. In: Proceedings of the US EPA/NGWA Fractured Rock Conference, Portland, pp. 882–894.

Dowd, P., Xu, C., Mardia, K., Fowell, R., 2007. A comparison of methods for the stochastic simulation of rock fractures. Mathematical Geology 39 (7), 697–714.

d'Alessio, M., Martel, S., 2004. Fault terminations and barriers to fault growth. Journal of Structural Geology 26, 1885–1896.

Freudenreich, Y., del Monte, A., Angerer, E., Reiser, C., Glass, C., 2005. Fractured reservoir characterisation from seismic and well analysis: a case study. In: 67th EAGE Conference & Exhibition, Madrid, Spain, 13–16 June, pp. 1–4.

Gringarten, E., 1998. FRACNET: stochastic simulation of fractures in layered systems. Computers & Geosciences 24 (8), 729–736.

Hoffmann, W., Dunne, W., Mauldon, M., 2004. Probabilistic–mechanistic simulation of bed-normal joint patterns. In: Cosgrove, J., Engelder, T. (Eds.), The Initiation, Propagation and Arrest of Joint and Other Fractures. Geological Society, vol. 231. Special Publication, London, pp. 269–284.

Jing, L., 2003. A review of techniques, advances and outstanding issues in numerical modelling for rock mechanics and rock engineering. International Journal of Rock Mechanics & Mining Sciences 40, 283–353.

Kim, Y.-S., Peacock, D., Sanderson, D., 2004. Fault damage zones. Journal of Structural Geology 26, 503–517.

Kloppenburg, A., Alzate, J., Charry, G., 2003. Building a discrete fracture network based on the deformation history: a case study from the Guaduas Field, Colombia. In: The Eighth Simposio Bolivariano, Cartagena, Colombia, 21–24 September, pp. 1–4.

Macé, L., June 2006. Caractérisation et modélisation numérique tridimensionnelles des réseaux de fractures naturelles: application au cas des réservoirs. Ph.D. Thesis, Institut National Polytechnique de Lorraine.

Macé, L., Souche, L., Mallet, J.-L., October 2004. 3D fracture modeling integrating geomechanics and geologic data. In: AAPG International Conference & Exhibition, Cancun, Mexico, pp. 1–6.

Maerten, L., Pollard, D., Karpuz, R., 2000. How to constrain 3-D fault continuity and linkage using reflection seismic data: a geomechanical approach. AAPG Bulletin 84 (9), 1311–1324.

Olson, J., 1993. Joint pattern development: effects of subcritical crack growth and mechanical crack interaction. Journal of Geophysical Research 98 (B7), 12251–12265.

Pollard, D., Aydin, A., 1988. Progress in understanding jointing over the past century. Geological Society of America Bulletin 100, 1181–1204.

Priest, S., Hudson, J., 1976. Discontinuity spacings in rock. International Journal of Rock Mechanics and Mining Science & Geomechanics Abstracts 13, 135–148.

Renard, P., Straubhaar, J., Caers, J., Mariethoz, G., 2011. Conditioning facies simulations with connectivity data. Mathematical Geosciences 43, 879–903.

Renshaw, C., Pollard, D.D., 1994a. Are large differential stresses required for straight fracture propagation paths? Journal of Structural Geology 16 (6), 817–822.

Renshaw, C.E., Pollard, D.D., 1994b. Numerical simulation of fracture set formation: a fracture mechanics model consistent with experimental observations. Journal of Geophysical Research 99, 9359–9372.

Robinson, P.C., 1983. Connectivity of fracture systems—a percolation theory approach. Journal of Physics A: Mathematical and General 16 (3), 605–614.

Robinson, P.C., 1984. Numerical calculations of critical densities for lines and planes. Journal of Physics A: Mathematical and General 17, 23–28.

Scholz, C., Dawers, N., Yu, J., Anders, M., Cowie, P., 1993. Fault growth and fault scaling laws: preliminary results. Journal of Geophysical Research 98, 21951–21961.

Srivastava, R., Frykman, P., Jensen, M., 2005. Geostatistical simulation of fracture networks. In: Leuangthong, O., Deutsch, C.V. (Eds.), Geostatistics Banff 2004 of Quantitative Geology and Geostatistics, vol. 14. Springer, pp. 295–304.

Stoyan, D., Kendall, W., Mecke, J., 1995. Stochastic Geometry and its Applications. John Wiley & Sons, New York.

Tuckwell, G., Lonergan, L., Jolly, R., 2003. The control of stress history and flaw distribution on the evolution of polygonal fracture networks. Journal of Structural Geology 25 (August (8)), 1241–1250.

Vermilye, J., Scholz, C., 1998. The process zone: a microstructural approach view of fault growth. Journal of Geophysical Journal B: Solid Earth 103 (B6), 12223–12237.

Welch, J., Davies, R., Knipe, R., Tueckmantel, C., 2009. A dynamic model for fault nucleation and propagation in mechanically layered section. Tectonophysics 474, 473–492.

Will, R., Archer, R., Dershowitz, B., 2004. A discrete fracture network approach to conditioning petroleum reservoir models using seismic anisotropy and production dynamic data. In: SPE Annual Technical Conference and Exhibition (SPE 90487), Houston, Texas, USA, 26–29 September, pp. 2843–2857.